Computerized Medical Imaging and Graphics 88 (2021) 101845

Contents lists available at ScienceDirect

Computerized Medical Imaging and Graphics

journal homepage: www.elsevier.com/locate/compmedimag

A deep learning approach to the screening of malaria infection: Automated and rapid cell counting, object detection and instance segmentation using Mask R-CNN

De Rong Loh [a,1], Wen Xin Yong [b,1], Jullian Yapeter [c], Karupppasamy Subburaj [b,**], Rajesh Chandramohanadas [b,d,*,2]

[a] Pillar of Information Systems Technology and Design, Singapore University of Technology and Design, Singapore, Singapore
[b] Pillar of Engineering Product Development, Singapore University of Technology and Design, Singapore, Singapore
[c] Faculty of Engineering, University of Waterloo, Ontario, Canada
[d] Department of Microbiology and Immunology, National University of Singapore, Singapore

ARTICLE INFO

Keywords:
Malaria diagnosis
Mask R-CNN
Computer vision
Image analysis

ABSTRACT

Accurate and early diagnosis is critical to proper malaria treatment and hence death prevention. Several computer vision technologies have emerged in recent years as alternatives to traditional microscopy and rapid diagnostic tests. In this work, we used a deep learning model called Mask R-CNN that is trained on uninfected and *Plasmodium falciparum*-infected red blood cells. Our predictive model produced reports at a rate 15 times faster than manual counting without compromising on accuracy. Another unique feature of our model is its ability to generate segmentation masks on top of bounding box classifications for immediate visualization, making it superior to existing models. Furthermore, with greater standardization, it holds much potential to reduce errors arising from manual counting and save a significant amount of human resources, time, and cost.

1. Introduction

Malaria is a life-threatening disease caused by *Plasmodium* parasites that are transmitted through the bites of infected female Anopheles mosquitoes to humans. The most common and severe form of malaria is caused by the species *Plasmodium (P.) falciparum*. Notably, *P. falciparum* is responsible for at least 76 % of estimated malaria cases in the WHO African Region, as well as in the other WHO regions of South-East Asia (52 %), the Eastern Mediterranean (75 %) and the Western Pacific (66 %). Children under 5 years old are the most vulnerable and affected, accounting for more than 60 % of all malaria deaths worldwide (W. H. Organization, 2018).

Since an effective vaccine against malaria has yet to be developed, an affordable, accurate and timely diagnosis is necessary and must be accessible in resource-poor settings, in order to prevent the development of severe malaria as well as onward transmission. Due to the success in using machine learning models for computer-aided disease diagnosis, many researchers have explored the use of Deep Learning models to automate the screening and detection process for Malaria, and they were able to achieve results with high accuracy (Fuhad et al., 2020; Poostchi et al., 2018a; Rahman et al., 2019). However, the classification of life stages of the Malaria parasite is often not identified, and it is vital to identify and highlight the life stages during the diagnosis as they represent disease severity and therefore affect the efficacy of the treatment (Delves et al., 2012). In this paper, we will explore the use of the Mask R-CNN model, which is capable of object detection and classification, as an alternative method for automated Malaria screening (He et al., 2017).

1.1. Diagnostic options

Light microscopy and Rapid Diagnostic Tests (RDTs) are the two

* Corresponding author at: Department of Microbiology & Immunology, National University of Singapore, 5 Science Drive 2, 117545, Singapore.
** Corresponding author.
E-mail addresses: derong_loh@mymail.sutd.edu.sg (D.R. Loh), wenxin_yong@mymail.sutd.edu.sg (W.X. Yong), jullian.yapeter@uwaterloo.ca (J. Yapeter), subburaj@sutd.edu.sg (K. Subburaj), micrc@nus.edu.sg, rajesh@sutd.edu.sg (R. Chandramohanadas).
[1] These authors contributed equally.
[2] http://epd.sutd.edu.sg/faculty/rajesh-chandramohanadas/.

https://doi.org/10.1016/j.compmedimag.2020.101845
Received 19 July 2020; Received in revised form 1 December 2020; Accepted 11 December 2020
Available online 12 January 2021

most widely used diagnostic means in remote malaria-affected regions, with the former being the current gold standard for clinical malaria diagnosis (Keiser et al., 2002). However, several inherent disadvantages make the light microscopy-based diagnosis an undesirable option. Firstly, extensive training is required for a microscopist to be proficient in slide reading. Secondly, there is a lack of standardization due to the differences in the experience and skill of the microscopists (Poostchi et al., 2018b). Furthermore, they tend to work in isolation without any rigorous quality control and monitoring system to ensure diagnostic accuracy and reproducibility, risking inappropriate treatment decisions. For example, false negatives and false positives lead to unnecessary use of antibiotics and antimalarial drugs, respectively, which can lead to progressive drug resistance. Thirdly, the time required and overwhelming workload lead to high cost, given the fact a single comprehensive microscopic examination takes 15−30 min for a trained microscopist, and that there are thousands of blood slides to be manually inspected every year (Poostchi et al., 2018b).

RDTs, though slightly faster and require only minimal training, are more expensive in high-burden areas and do not quantify the results, which is needed to serve as a prognostic indicator (Poostchi et al., 2018b; W. H. Organization, 2021). RDTs may also fail to detect infections with low parasite density (Rosado et al., 2017). Crucially, its use has not eliminated the need for microscopy, but is instead viewed as complementary. Other methods such as Polymerase Chain Reaction (PCR) technique, flow cytometry, and fluorescence microscopy are not suitable to be deployed in the field due to their inability to meet certain criteria such as cost per test and required skill level of the user (Poostchi et al., 2018b).

1.2. Mask R-CNN as an alternative

Deep Neural Network (DNN), which is one of the many algorithms used in Machine Learning, is commonly adopted to solve difficult real-life problems (Miotto et al., 2017; Razzak et al., 2018). Within the DNN architecture, one of its forms, Convolutional Neural Network (CNN), is the popular and the most influential architecture in computer vision due to its superior capability to perform image analysis (Bote--Curiel et al., 2019; Cao et al., 2018; Yao et al., 2019). Its capability to process and analyze a large number of images opens new possibilities in the medical field, which has proven to increase the efficiency and accuracy of image analysis in cell biology experiments (Yao et al., 2019; Xu et al., 2017). Another advantage of CNN is the modularity and flexibility of the architecture, where the pre-trained network can be reused and improvised with the related labelled images to suit additional features through Transfer Learning (Bote-Curiel et al., 2019). Recently, it was found that CNN is widely researched and applied in the medical imaging field (Cornell Engineering, 2021) due to its promising performance in detecting lesions and abnormalities (Razzak et al., 2018; Khosravan and Bagci, 2018).

In recent years, CNN has progressively evolved into more sophisticated forms. Researchers have used Faster R-CNN to localize and classify malaria-infected cells (Hung et al., 2018). The localization feature of Faster R-CNN yields bounding boxes around each cell of interest. Especially with a field that is densely populated with cells, coarse bounding boxes can result in overcrowded images with confusing overlapping of boxes. Mask R-CNN addresses this potential issue using pixel-wise masking, which provides a fine distinction between the boundaries of cells and thus allows medical professionals to more confidently pair up the cells to their corresponding predicted classification.

CNN has progressively evolved into more sophisticated forms, such as R-CNN and Faster R-CNN, both of which are capable of robust object detection, as well as Mask R-CNN that can be used for instance segmentation steps. Not only that, Mask R-CNN has also surpassed all previous state-of the-art single-model results on the COCO instance segmentation task (He et al., 2017). Hence, we propose using a *P. falciparum* trained Mask R-CNN model to automatically detect and quantify cells at different stages quickly and accurately in a bid to improve the diagnostic process, especially in resource-poor settings (He et al., 2017).

2. Materials and methods

2.1. Blood collection and parasite culture

Human blood for culturing *Plasmodium* was purchased from Interstate blood bank (USA). *Plasmodium falciparum*, 3D7 strain was used for all experiments reported in this work. Parasites cultured in human RBCs under standard conditions (Subramanian et al., 2016) were smeared on glass slides, fixed with methanol and stained with 1:10 diluted Giemsa solution (Merck, Singapore) for microscopic examinations and phenotypic determination. Images were captured using a Leica digital camera connected to a Leica ICC50 W microscope, as reported in prior work (Subramanian et al., 2018).

2.2. Dataset splitting and labelling

Our dataset consists of 297 images, of which 173 were used for training, 64 for validation, and 60 for testing in an approximate ratio of 3:1:1. The images were manually annotated using the online VGG Image Annotator (VIA 2.0.4) before being exported as a json file, for the training phase (Dutta et al., 2021a). The polygon shape tool was used to trace out the borders, and regions of interest were then labelled accordingly based on the classification of the specific developmental stage of the parasite (Yang et al., 2017).

Out of the five classes identified, only four classes, which are uninfected reticulocyte, ring, trophozoite, and schizont, were labelled. Reticulocytes were included in the analysis, since anaemia resulting from malaria can lead to higher reticulocyte counts in blood smears and may have distinct staining pattern compared to mature normocytes. The uninfected normocyte class was intentionally excluded to save time on manual annotations due to a large number of healthy normocytes present in each smear.

Not all the classifications were straightforward. Firstly, some cells could be transitioning from one stage to another when the image was captured. A late trophozoite looks morphologically similar to an early schizont. Secondly, there were occasional multiple infections. Hence, we developed and adhered to a set of guidelines because the same model trained on our custom labelled dataset will be used for prediction as well.

Ring stages have a visible cytoplasm and 1 or 2 chromatin dots (Poostchi et al., 2018b). Trophozoites have denser cytoplasm with brown malarial pigment (hemozoin) present inside. Schizonts are larger than trophozoites, where we set an arbitrary threshold of 60 % parasite occupancy in the infected red blood cell. Typically, during late stages, distinct nuclei (newly formed merozoites) can be observed with hemozoin clumped together. The label will follow the later stage for rare cases of multiple infections by parasites belonging to different stages.

2.3. Transfer learning

The transfer learning technique was applied to an existing Mask R-CNN model developed by Matterport (2021), with modifications made to suit our custom labelled dataset (Fig. 1). Briefly, the region proposal network was applied to the extracted feature maps, which returned the ROIs and their associated scores. Following which the ROI Align layer was used to accurately map the original image to the feature map, where the outputs were processed in parallel to predict binary mask and bounding coordinates. Weight initialization was performed using the pre-trained weights of the model that was trained on the COCO dataset (Lin et al., 2021). All operations were done in the Google Colaboratory environment (Dutta et al., 2021b).

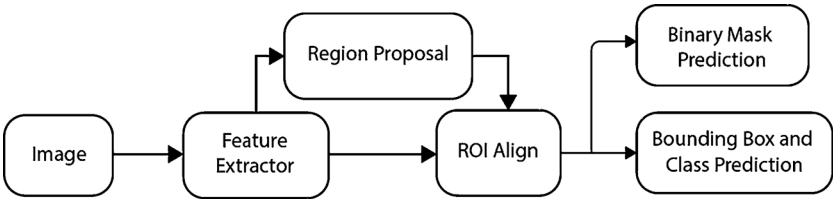

Fig. 1. Mask R-CNN Architecture. The final outputs are bounding boxes with class predictions for Object Detection, and a selective binary mask for Instance Segmentation.

The prediction of the input image primarily involved three stages. In the first stage, region proposals were generated, followed by running classifier heads on the region proposals to generate class probabilities and bounding box regressions. The minimum confidence level for detection was set at 80 %, filtering away identified targets with lower ROI scores. In the third stage, the mask head was run on the detections to generate a segmentation mask for every instance.

2.4. Cell counting algorithm

Since the healthy normocyte class was not labelled, we included a cell counting algorithm to estimate the total number of cells. The healthy normocyte number is estimated by subtracting the total number of cells with the other four classes predicted by our model, as shown in the following equation:

Healthy (uninfected) Normocytes = Total Cells – Uninfected Reticulocytes – Rings – Trophozoites – Schizonts

We also modified the algorithm to be able to output corresponding selective masks for each class as well as work on predicting unseen test images.

Image processing techniques from *cv2* and *scikit*-image were employed in the cell counting algorithm (Bradski, 2000; Van der Walt et al., 2014). With the given image, its contrast was improved by applying histogram equalisation on lightness colour space of the image (Histogram equalization, 2021). Then, a threshold binary function was applied to the blurred and edge-smoothened image to separate the cells from the background (Basic thresholding operations, 2021). Morphological operations, such as opening and erosion, were performed to remove noise (Morphological transformations, 2021). In addition to optimizing the number of morphological operations used, non-maximum suppression thresholds as well as min confidence levels were employed to be more selective in identifying regions and bounding boxes for the cells. The watershed algorithm was then used to segment each cell. Finally, the total number was counted (Watershed segmentation, 2021).

2.5. Model evaluation

The model's performance was evaluated by comparing its predictions with the number of stage-specific cells counted independently by two researchers with more than 5 years of experience with counting plasmodium-infected RBCs. Specifically, confusion matrix and mean average precision (mAP) were used as the standard metrics for object detection. With reference to Fig. 3, the parameters for the confusion matrix are defined by the following formulas:

$$Accuracy\ \ in\ \ detecting\ \ cells = \frac{Cluster\ \ A\ +\ Cluster\ \ B}{Cluster\ \ A\ +\ Cluster\ \ B\ +\ Cluster\ \ C}$$

$$Accuracy\ \ in\ \ labelling\ \ infected\ \ cells = \frac{Cluster\ \ A}{Cluster\ \ A\ +\ Cluster\ \ B\ +\ Cluster\ \ C}$$

$$Error\ \ on\ \ labelling\ \ infected\ \ cells = \frac{Cluster\ \ C\ +\ Cluster\ D}{Total\ \ Manual\ \ Cell\ \ Count}$$

The overall mAP was calculated by taking the average of the calculated 11-point interpolated AP score of each class based on the precision and recall values with an IoU threshold value of 0.5. The model used in our study is available at the link: https://github.com/sutdteam/malaria_mask_rcnn.

3. Results

3.1. Object detection and instance segmentation

The trained model was able to identify all the cells of interest successfully and perform object detection accurately as evident from the bounding boxes (Fig. 2B). The associated class probabilities were also consistently high (close to 1) and correct, suggesting that the prediction was exact.

In a parallel branch, the model was also capable of producing segmenting masks (Fig. 2C–F). This allowed easy and clear visualisation of the spatial locations of cells in their respective stages, which could potentially be useful in monitoring disease progression. Notice that in Fig. 2C, there were no uninfected reticulocytes present in the original image, hence the output was simply a grey segmenting mask.

3.2. Object detection metrics

The confusion matrix (Table 1) provided data to calculate the results for Figs. 3 and 4. Based on Table 2 and Fig. 3, the model achieved 94.57 % accuracy in detecting infected cells with 0.55 % error, 82 % accuracy in labelling given that the cell was infected. The high accuracy value was also corroborated by the high percentages of true positives where most of the infected cells were correctly predicted as their true respective stages (Fig. 4).

The cell counting algorithm also showed positive results (Table 2), with a tolerable total cell count difference of 10 %, implying that the overall cell counts were reasonably accurate. The difference could be attributed to the inability of the algorithm to segment overlapping cells that lacked a definite boundary.

The overall mAP was evaluated to be 0.731 by taking the average of the 11-point interpolated AP of all 4 labelled classes: ring (0.649), trophozoite (0.462), schizont (0.814) and reticulocyte (1.000). Almost all the ROI proposals were generated with high IoU values with the Ground Truth ROIs as evident from the tight boxes around the cell boundaries. Thus, we consider our obtained mAP value to be satisfactory as this score would not drop drastically even at higher IoU threshold values.

3.3. Comparison with other existing models

On identifying infected cells, we compared the test accuracy of our Mask R-CNN model with existing models (Table 3).

In Table 4, we further compared the stage-specific error margins of our trained Mask R-CNN model and its predecessor, the Faster R-CNN model, by expressing the absolute difference between the predicted and

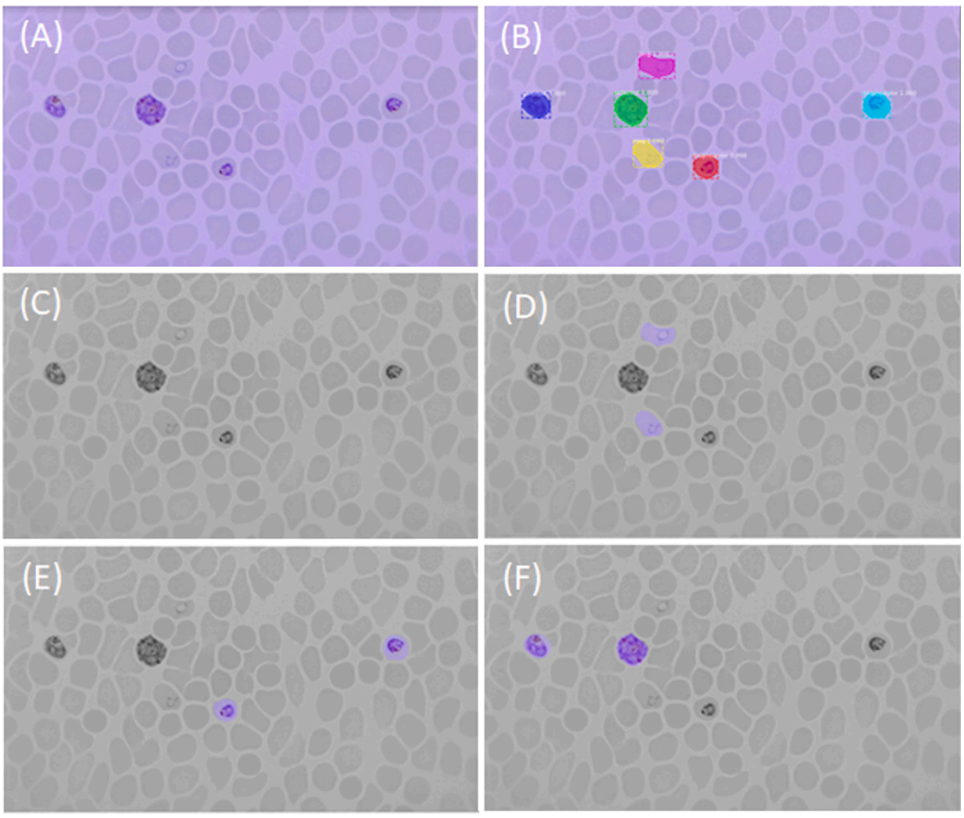

Fig. 2. Images automatically analysed by the Mask R-CNN model.
(**A**) Original image taken by immersion objective 100×.
(**B**) Bounding box classifications and class probabilities for all extracted uninfected reticulocytes and iRBCs.
(**C-F**) Selective mask for extracted stages in the following order: Uninfected Reticulocyte, Ring, Trophozoite, and Schizont.

Table 1
Confusion Matrix. The confusion matrix targets only the infected cells in the 60 images.

		Predicted cell types				
		Normocyte	Ring	Trophozoite	Schizont	Uninfected Reticulocyte
Actual cell types (verified through microscopy)	Normocyte	0	15	0	1	6
	Ring	17	92	1	0	4
	Trophozoite	5	22	98	15	0
	Schizont	11	1	49	384	1
	Uninfected Reticulocyte	0	0	0	0	11

actual counts (derived from the ground truth) as a percentage of the actual cell counts.

4. Discussion

Efficient and accurate classification and diagnosis of infected cells are critical to make appropriate clinical decisions, including prescribing treatment and monitoring progress. In this work, we have developed and tested a deep learning based model to segment, classify, and count *Plasmodium falciparum*-infected red blood cells. Testing results suggest that our model is accurate, 15 times faster, and inexpensive to operate, as compared to the current gold standard of manual counting. Considering the model has been trained already, test images can be uploaded to obtain segmentation masks (Fig. 2) and parasitemia report (Fig. 5) for downstream processing.

The accuracy of our model is also comparable to the reported models in the literature (Table 3). In particular, our model demonstrated a significant improvement over the antecedent Faster R-CNN model. Despite operating at a higher minimum confidence threshold value of 0.8, as compared to 0.65 in the One Stage Faster R-CNN model, our model is able to predict ring and schizont cell stages with a smaller error margin, as seen from Table 4.

The schizont class had a high AP score of 0.841 because a significant number of true positives was correctly predicted at high confidence levels, despite being heavily penalized by a considerable number of false negatives due to the aforementioned reasons. Its relatively higher score can be attributed to its larger sample sizes in the dataset. The uninfected reticulocyte class had a perfect AP score of 1 because all the false positives were detected at a lower confidence level than the true positives, albeit with a limited sample size, which must be considered when interpreting the result.

Upon closer inspection and comparison of the labelled results predicted by our model and the microscopists, most misclassifications were caused by the ambiguities in stage transitions, as shown in Fig. 4. In particular, the trophozoite class expectedly had the lowest AP score due to uncertainties in both the ring-trophozoite and the trophozoite schizont stage transitions. The model's performance was also penalized by several clearly misclassified and unlabelled data points by the microscopists.

According to the six selected criteria, our model has outperformed traditional manual counting (Table 5). Our model does not require a trained microscopist. Such skill specialization is not easily available in

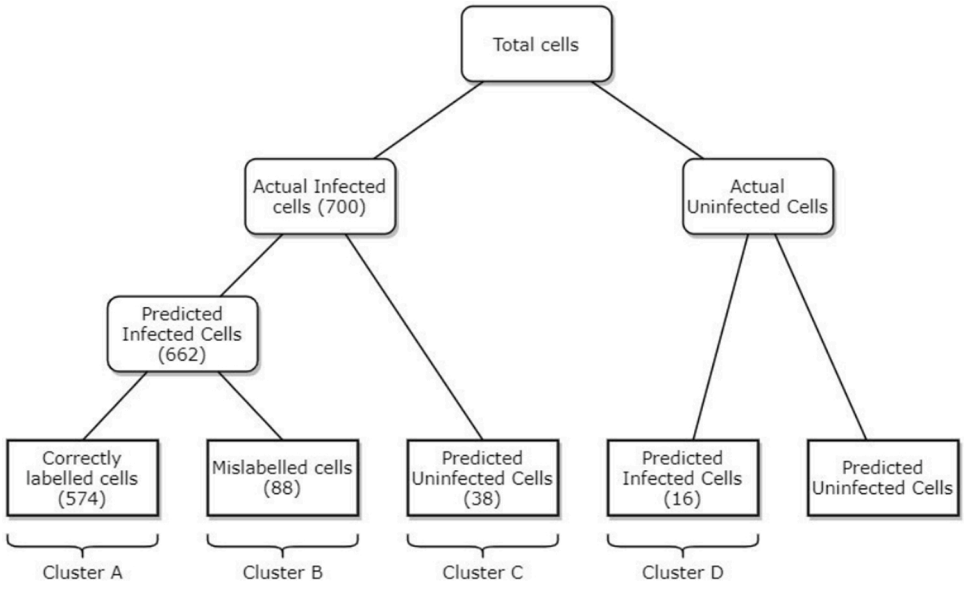

Fig. 3. Derived tree from Confusion Matrix in Table 1. Actual normocyte counts were omitted as it was not one of the labeled datasets.

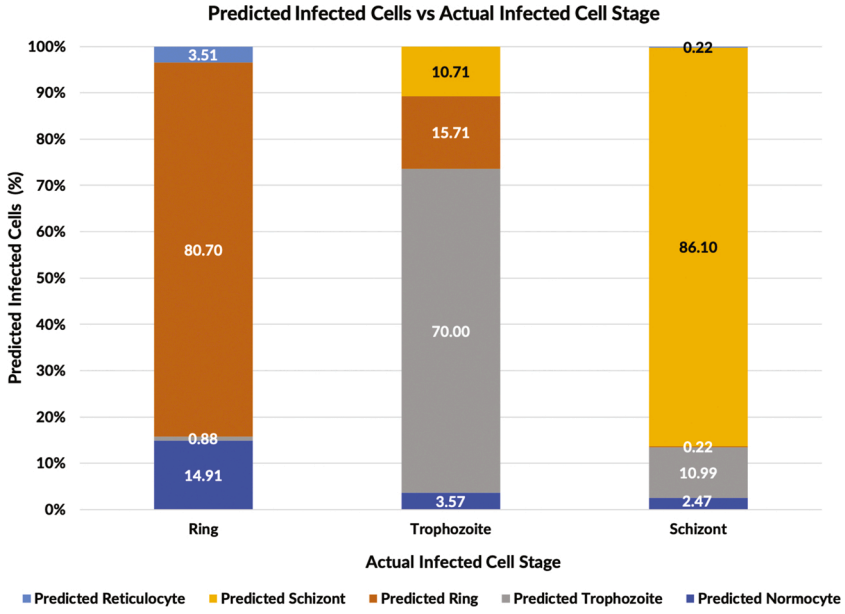

Fig. 4. Bar Chart of True Results v.s. Percentage of Predicted Results.

Table 2
Result of the Cell Counting Algorithm.

Method	Total Cell Count	Difference (%)
Manual Counting	6908	10.44
Cell Counting Algorithm	6187	

Table 3
Comparison with other existing models.

Model	Test Accuracy (%)
Custom (Rahman et al., 2019)	96.29
TL-VGG16 (Rahman et al., 2019)	97.77
State-of-the-art Customized (Rahman et al., 2019)	94.00
State-of-the-art ResNet-50 (Rahman et al., 2019)	95.70
CNNEx-SVM (Rahman et al., 2019)	94.77
One Stage Faster R-CNN Detection (Hung et al., 2018)	59.00
Two Stage Detection (Hung et al., 2018)	98.00
Mask R-CNN	94.57

resource-poor settings, and training professionals is time- and resource-intensive. Our model is able to produce a highly accurate, reproducible and comprehensive report including individual and overall cell counts more quickly, taking only 4 s on an average to process each image. On the other hand, manual counting takes a full conservative minute per image, with accuracy and productivity decreasing over time.

In terms of scalability, our model is capable of handling more classes to potentially include other types of cells relevant to malaria infection and immune response, such as gametocytes and leukocytes, and associated diseases as long as there are sufficient well-annotated images for training purposes. Unlike many existing computer-vision algorithms, we have demonstrated that our model can detect subtle and less-

Table 4
Comparison by each stage with Faster R-CNN.

Class	Error Margin (%)	
	One Stage Faster R-CNN	Mask R-CNN
Ring	157.95	5.15
Trophozoite	18.36	27.41
Schizont	39.28	11.72

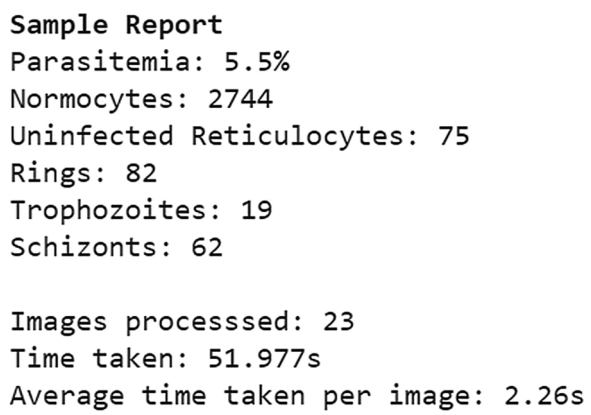

Fig. 5. Sample Report. It shows the overall cell counts in each stage and the parasitemia values for malaria diagnosis.

Table 5
Metrics Scoring of our Mask R-CNN model, as compared with Manual Counting. Our model fares better than traditional manual counting method in all six critical criteria.

	Mask R-CNN	Manual Counting
Accuracy	82.00 %	Varies between individuals Decreases greatly over long working hours
Consistency	Standardized and reproducible results	
Skill level	Not required	Only trained microscopists allowed
Time	4s per image	120 s per image
Cost	Electricity fees	Manpower and time
Scalability	Can include other species and diseases	Not applicable

common differences between parasitic stages. For example, despite limited dataset for uninfected reticulocytes, our model was still able to distinguish them from infected mature red blood cells, which would not have been possible using the average pixel intensity algorithm (Yang et al., 2017). This distinction is useful information considering that *P. falciparum* infects both reticulocytes and mature red blood cells, and some species are restricted solely to reticulocytes.

Computer vision technologies hold enormous potential in creating a unified platform for medical diagnosis in resource-poor regions. As a comparison, to achieve the same feat, it would be highly impractical to train every microscopist to be as skilled in differentiating different types of cells and diseases.

5. Future work

As a proof of concept, we have shown that deep learning can be applied to a custom malaria dataset and demonstrated a well-trained Mask R-CNN model as a promising first-stage classification tool in reducing this global health problem. Moving forward, we intend to improve this model with a larger dataset, or with an additional stage of classification (Hung et al., 2018), and eventually incorporate it into an AI-powered automated microscope in order to achieve a more reliable and faster screening process. We also hope that our work can inspire the creation of a unified platform for medical diagnosis in regions with poor resources by expanding the number of classes to include other types of cells and diseases.

To improve the system further, we aim to use synchronization techniques to control the RBCs' infection period classification and fine-grain our labelling approach during the training to reduce bias. We explore semi-automated methods for tagging and labelling before counting them and facilitate batch processing to reduce time and effort. Considering the cells' borders in our images have good contrast, instead of labelling each cell's perimeters, a few pixels could be labelled to perform the image segmentation (Graph Cut algorithm (Beheshti et al., 2015)) by training the Mask R-CNN. Also, include the possibility to capture larger areas of blood smears (and therefore more parasites/frame). We intend to deploy quality check measures, including cells with a high intersection over-union (IoU) ratio (Toda et al., 2020), to make sure the smear images have less overlapped or aggregated RBCs before proceeding with the downstream analysis. To reduce performance variations due to image scaling, we propose to utilize the multiscale image pyramids method (Kang and Chan, 2018) to perform object detection in a series of up-sampled images and then fuse them. Considering that RBCs' overlap is inherently a small feature compared to the cells, upsampling would make the overlap more apparent and detectable.

CRediT authorship contribution statement

De Rong Loh: Conceptualization, Software, Formal analysis, Data curation, Writing - original draft. **Wen Xin Yong:** Conceptualization, Software, Formal analysis, Data curation, Writing - original draft. **Jullian Yapeter:** Conceptualization, Software, Formal analysis, Data curation. **Karupppasamy Subburaj:** Investigation, Methodology, Resources, Software, Supervision, Writing - review & editing. **Rajesh Chandramohanadas:** Conceptualization, Funding acquisition, Formal analysis, Project administration, Resources, Supervision, Writing - review & editing.

Declaration of Competing Interest

The authors report no declarations of interest.

Acknowledgements

We would like to thank Drs. Gowtham Subramaniam and Renugah Naidu for providing us with the Giemsa-stained slides for image capturing and helping out with the cell counting. We would like to express our gratitude toward Singapore University of Technology and Design (SUTD) Undergraduate Research Opportunities Programme (UROP00748) for partially funding this research.

Appendix A. Supplementary data

Supplementary material related to this article can be found, in the online version, at doi:https://doi.org/10.1016/j.compmedimag.2020.101845.

References

Basic thresholding operations. https://docs.opencv.org/2.4/doc/tutorials/imgproc/threshold/threshold.html.
Beheshti, M., Faichney, J., Gharipour, A., 2015. Bio-cell image segmentation using bayes graph-cut model. 2015 International Conference on Digital Image Computing: Techniques and Applications (DICTA) 1–5.

Bote-Curiel, L., Muñoz-Romero, S., Gerrero-Curieses, A., Luis Rojo-Álvarez, J., 2019. Deep learning and big data in healthcare: A double review for critical beginners. Appl. Sci. 9 (June).

Bradski, G., 2000. The OpenCV library. Dr. Dobb's J. Softw. Tools 25, 120–125.

Cao, C., Liu, F., Tan, H., Song, D., Shu, W., Li, W., Zhou, Y., Bo, X., Xie, Z., 2018. Deep learning and its applications in biomedicine. Genomics Proteomics Bioinformatics 16 (03).

Cornell Engineering, 2021. Computer Vision. http://www.via.cornell.edu/research/overview.html.

Delves, M., Plouffe, D., Scheurer, C., Meister, S., Wittlin, S., Winzeler, E.A., Sinden, R.E., Leroy, D., 2012. The activities of current antimalarial drugs on the life cycle stages of plasmodium: a comparative study with human and rodent parasites. PLoS Med. 9 (2).

Dutta, Abhishek, Gupta, Ankush, Zisserman, Andrew, 2021a. VGG Image Annotator (VIA). https://www.robots.ox.ac.uk/~vgg/software/via/.

Dutta, Abhishek, Gupta, Ankush, Zisserman, Andrew, 2021b. Google Colaboratory.

Fuhad, K.M.F., Tuba, J.F., Sarker, M.R.A., Momen, S., Mohammed, N., Rahman, T., 2020. Deep learning based automatic malaria parasite detection from blood smear and its smartphone based application. Diagnostics 10 (5), 329.

He, K., Gkioxari, G., Dollár, P., Girshick, R.B., 2017. Mask R-CNN. CoRR abs/1703.06870.

Histogram equalization. https://docs.opencv.org/2.4/doc/tutorials/imgproc/histograms/histogram_equalization/histogram_equalization.html.

Hung, J., Goodman, A., Lopes, S., Rangel, G., Ravel, D., Costa, F., Duraisingh, M., Marti, M., Carpenter, A.E., 2018. Applying faster R-CNN for object detection on malaria images. CoRR abs/1804.09548.

Kang, D., Chan, A.B., 2018. Crowd counting by adaptively fusing predictions from an image pyramid. CoRR abs/1805.06115.

Keiser, J., Utzinger, J., Premji, Z., Yamagata, Y., Singer, B., 2002. Acridine orange for malaria diagnosis: Its diagnostic performance, its promotion and implementation in tanzania, and the implications for malaria control. Ann. Trop. Med. Parasitol. 96 (11), 643–654.

Khosravan, N., Bagci, U., 2018. S4nd: single-shot single-scale lung nodule detection. CoRR abs/1805.02279.

Tsung-Yi Lin, Genevieve Patterson, Matteo R. Ronchi, Yin Cui, Michael Maire, Serge Belongie, Lubomir Bourdev, Ross Girshick, James Hays, Pietro Perona, Deva Ramanan, Larry Zitnick, Piotr Dollár, "Common Object in Context (COCO)." https://ddec1-0-en-ctp.trendmicro.com:443/wis/clicktime/v1/query?url=http%3a%2f%2fcocodataset.org&umid=697e4cc8-4138-4f4d-ac8d-1f6d7cba19bc&auth=8d3ccd473d52f326e51c0f75cb32c9541898e5d5-ff1e61a268c51eb58ca9481d828f61b69134e648#home.

Matterport, 2021. Mask R-CNN for Object Detection and Segmentation. https://github.com/matterport/Mask_RCNN.

Miotto, R., Wang, F., Wang, S., Jiang, X., Dudley, J.T., 2017. Deep learning for healthcare: review, opportunities and challenges. Brief. Bioinformatics 19 (June), 1236–1246.

Morphological transformations. https://docs.opencv.org/trunk/d9/d61/tutorial_py_morphological_ops.html.

Poostchi, M., Silamut, K., Maude, R.J., Jaeger, S., Thoma, G., 2018a. Image analysis and machine learning for detecting malaria. Transl. Res. 194, 36–55.

Poostchi, M., Silamut, K., Maude, R.J., Jaeger, S., Thoma, G., 2018b. Image analysis and machine learning for detecting malaria. Transl. Res. 194, 36–55. In-Depth Review: Diagnostic Medical Imaging.

Rahman, A., Zunair, H., Rahman, M.S., Yuki, J.Q., Biswas, S., Alam, M.A., Alam, N.B., Mahdy, M., 2019. Improving malaria parasite detection from red blood cell using deep convolutional neural networks. ArXiv abs/1907.10418.

Razzak, M.I., Naz, S., Zaib, A., 2018. Deep Learning for Medical Image Processing: Overview, Challenges and the Future. Springer International Publishing, Cham, pp. 323–350.

Rosado, L., Correia da Costa, J.M., Elias, D., Cardoso, J., 2017. Mobilebased analysis of malaria-infected thin blood smears: Automated species and life cycle stage determination. Sensors 17 (09), 2167.

Subramanian, G., Rajeev, C.B., Mohan, C.D., Sinha, A., Chu, T.T., Anusha, S., Ximei, H., Fuchs, J.E., Bender, A., Rangappa, K.S., Chandramohanadas, R., Basappa, 2016. Synthesis and in vitro evaluation of hydrazinyl phthalazines against malaria parasite, plasmodium falciparum. Bioorg. Med. Chem. Lett. 26 (14), 3300–3306.

Subramanian, G., Belekar, M.A., Shukla, A., Tong, J.X., Sinha, A., Chu, T.T.T., Kulkarni, A.S., Preiser, P.R., Reddy, D.S., Tan, K.S.W., Shanmugam, D., Chandramohanadas, R., 2018. Targeted phenotypic screening in plasmodium falciparum and toxoplasma gondii reveals novel modes of action of medicines for malaria venture malaria box molecules. mSphere 3 (1).

Toda, Y., Okura, F., Ito, J., Okada, S., Kinoshita, T., Tsuji, H., Saisho, D., 2020. Training instance segmentation neural network with synthetic datasets for crop seed phenotyping. Commun. Biol. 3, 173, 04.

Van der Walt, S., Schönberger, J.L., Nunez-Iglesias, J., Boulogne, F., Warner, J.D., Yager, N., Gouillart, E., Yu, T., 2014. scikit-image: image processing in python. PeerJ 2, e453.

W. H. Organization, 2018. World Malaria Report 2018. Nov.

W. H. Organization, 2021. Determining Cost Effectiveness of Malaria Rapid Diagnostic Tests in Rural Areas with High Prevalence.

Watershed segmentation. https://scikit-image.org/docs/dev/auto_examples/segmentation/plot_watershed.html.

Xu, M., Papageorgiou, D., Abidi, S., Dao, M., Zhao, H., Karniadakis, G., 2017. A deep convolutional neural network for classification of red blood cells in sickle cell anemia. PLoS Comput. Biol. 13 (10), e1005746.

Yang, D., Subramanian, G., Duan, J., Gao, S., Bai, L., Chandramohanadas, R., Ai, Y., 2017. A portable image-based cytometer for rapid malaria detection and quantification. PLoS One 12 (06), 1–18.

Yao, K., Rochman, N., Sun, S., 2019. Cell type classification and unsupervised morphological phenotyping from low-resolution images using deep learning. Sci. Rep. 9 (09), 1–13.